

Dynamics of small domain-wall oscillations. Magnetic distribution in iron-garnet films

L. V. Velikov, E. P. Lyashenko, and S. S. Markianov

P. N. Lebedev Physics Institute, USSR Academy of Sciences

(Submitted 13 August 1982)

Zh. Eksp. Teor. Fiz. **84**, 783–791 (February 1983)

Results are presented of experimental investigations of the spectra of small oscillations of domain walls in thin films of mixed iron garnets, carried out using a specially developed highly sensitive magneto-optical equipment with a calibrated-photoreceiver bandwidth 31 MHz. The characteristic dispersion observed in the low-frequency region of the spectra (0.5–1.0 MHz) is attributed to a magnetic aftereffect interpreted within the framework of the induced-anisotropy model and leading to stabilization of the domain walls by the induced potential barriers and to additional energy dissipation when the domain walls move. The measured time constants of the relaxation of the effect are of the order of 10^{-7} sec. The influence of the aftereffect on the distortion of the spectra of domain-wall relaxation-type oscillations due to Landau-Lifshitz damping is discussed, as well as the apparent decrease of the domain-wall mobility on account of the shift of the effective relaxation frequency of the spectra.

PACS numbers: 75.70.Kw, 75.60.Lr, 75.60.Ch

1. INTRODUCTION

It is known that the dynamics of domain walls (DW) in weak fields is strongly influenced by interactions with various kinds of inhomogeneities and defects of the magnetic material,^{1–3} which lead to irreversible effects and to energy dissipation in the course of the DW motion. Besides such defects (pores, inclusions, etc.) the DW motion can be influenced also by magnetic-ion impurities and ion vacancies in the crystal lattices of mixed not-strictly-stoichiometric and doped compounds.^{4–9} If a domain structure is present in the crystal, the spatial inhomogeneity of the diffuse distribution of the impurity density in the vicinity of the DW gives rise, under the influence of the inhomogeneous orientation of the magnetic moment over its thickness, to an induced local anisotropy, and to the appearance of stabilizing potential barriers that pin the DW. For DW motion with low amplitudes, the kinetic processes of impurity relaxation leads to the so-called magnetic aftereffect and to dissipation of the DW energy. These are macroscopically observable as a supplementary dynamic coercivity of a DW in a certain range of its velocities.⁹ In the fast unidirectional displacements of a DW under the influence of stationary or pulsed fields, which are frequently used to investigate DW dynamics, both local microdefects of the material and the impurities make additive contributions to the irreversible effects and to the dissipation of the DW energy (coercivity), and from this point of view they are experimentally indistinguishable. However, in view of the finite rate of relaxation of the induced anisotropy due to the impurities, the magnetic aftereffects (MA) in the motion of DW have a specific frequency dispersion that can be experimentally observed and identified in measurements of the amplitude-frequency spectra of small DW oscillations under the influence of weak harmonic fields.

Investigations of broadband (0.1–15 MHz) spectra of small DW oscillations in thin films of mixed iron garnets with regular stripe-domain structure have revealed well-resolved regions of low-frequency dispersion, which are typi-

cal of MA. The measurements were made by photometric reading of the magneto-optic signal from the DW in the field-excitation frequency range from 0.1 to 15 MHz at DW oscillation amplitudes comparable with the DW width. The area of the sounded section of the sample was of the order of $100 \mu\text{m}^2$.

2. APPARATUS AND MEASUREMENT PROCEDURE

A highly sensitive setup for photometric of a magneto-optically modulated signal from a DW was developed for the measurement of the spectra of the DW oscillations. The setup is based on a polarization microscope equipped with high-aperture polarization Ahrens prisms. The necessary size of the sounded area of the sample can be set by the field and aperture diaphragms down to $10\text{-}\mu\text{m}$ diameter. The light source is an 400-watt illuminator with protective thermal light filters. The illuminator is fed through a current stabilizer with a three-stage LC filter that lowers the line ripple to 1 mV, and eliminates completely the synchronous noise at the output of the photomultiplier. The microcoil of the excitation field is fed through a matched cable from an oscillator with a low level of side harmonics. The most vital part of the setup is the photometric high-frequency head, since the task of the photoreceiving channel is to ensure a uniform and wide transmission band for the photomultiplier and calibration of the latter. We used in the setup a specially selected scintillation photomultiplier (FEU-55) with Venetian-blind dynode construction. An acceptable time-signal amplitude of the alternating signal on the matched load of the photomultiplier (75Ω) was ensured at anode currents 3–10 mA due to the constant background light flux from the sample. The photomultiplier high-voltage supply operated in a pulsed forced regime with stabilization of the voltage on the gap between the anode and the last dynode. The calibration of the photomultiplier intrinsic pass band was with the aid of broadband (100 MHz) electro-optical modulators and low-noise single-mode lasers for several values of the photo-

multiplier dc anode currents at light-beam modulation levels from 1.2 to 10%, close to the photomultiplier operating conditions in the setup. The measured intrinsic pass band of the photomultiplier was 31 MHz at the 0.4 level. Local irregularities and spikes of the amplitude-frequency characteristics, in the entire frequency band indicated for the given photomultiplier, did not exceed 2–3%. To prevent apparatus errors that were difficult to monitor, we dispensed with an electronic photomultiplier-signal dynamic-range expander used in Ref. 10. To separate the modulated signal, we used selective microvoltmeters with narrow pass band, in which case typical values of the signal/noise ratio for the investigated iron-garnet films were at the level 15–40. For bismuth-containing samples the signal/noise ratio increased to 50–80 and more.

Before measuring the frequency spectra of the DW oscillations, preliminary measurements were made of the static parameters of the sample: the period P_0 of the stripe-domain structure, the saturation magnetization $4\pi M_s$, the static initial susceptibility of the stripe structure $\chi_0 = 4\pi(\partial M/\partial H)$, and the structural susceptibility $\partial x/\partial H$ at low DW displacements, which is equal to the reciprocal gradient of the local demagnetizing field at the DW in the stripe structure. The function $l/h = f(P_0/h)$ tabulated in Ref. 11 was interpolated in the calculations of the characteristic length l over the period P_0 . To determine the remaining parameters, we plotted in the experiment the magnetization-curves of the sample with stripe-domain structure in a constant bias field by magnetic "loop-scope" method.¹² To this end we used the same photoreceiver head of the setup in a static regime, with the analyzer rotated 45°, to ensure linearity of the lux-ampere characteristic of the photomultiplier when measuring the relative magnetization $m = M/M_s$ of the sample. The magnetization curves $m(H)$ were recorded with an automatic x - y plotter. The parameter $\partial m/\partial H$ was determined from the initial slope of the magnetization curve, after which the structural susceptibility was calculated.

$$\partial x/\partial H = (\partial m/\partial H)P_0/4.$$

The relative susceptibility χ_0 was determined independently from the parameter l/h (Ref. 13):

$$\chi_0 = 4\pi M_s \frac{\partial m}{\partial H} \approx 1 + 7.14 \frac{l}{h},$$

and the saturation magnetization $4\pi M_s$ was calculated from χ_0 and corrected against the magnetization curve $m(H)$ using three points of the plot at the levels $m = 0.3, 0.5,$ and 0.8 . In

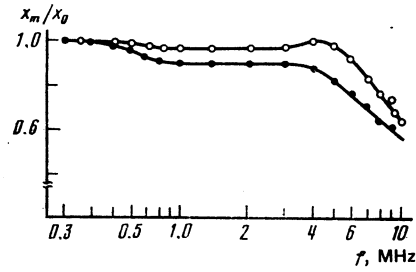


FIG. 1. General form of normalized typical amplitude-frequency spectra of DW oscillations in calcium-germanium iron-garnet films in the frequency range 0.1–12 MHz, with two different dispersion regions.

the measurements of $\partial m/\partial H$ a correction was introduced for the paramagnetic susceptibility of the substrate. The uniaxial-anisotropy field H_{er} was determined by a known procedure¹³ using a magneto-optic anisometer. The dynamic measurements were preceded by a preliminary "conditioning" of the stripe-domain structure by a weak low-frequency excitation field to obtain spatial stabilization of the structure and to eliminate irreversible Barkhausen jumps of the DW on possible macrodefects in the course of the spectrum measurements. The samples were nonimplanted epitaxial films of the garnets $(YSm)_3(FeGa)_5O_{12}$ and $(YSmCa)_3(FeGe)_5O_{12}$ from 3 to 12 μm thick. The film parameters are listed in Table I.

3. RESULTS AND DISCUSSION

The general form of the measured spectra of the DW oscillations is shown in Fig. 1, where two essentially different dispersion regions are clearly distinguishable: regions of HF dispersion with the relaxation falloff typical of viscous Landau-Lifshitz damping, located at frequencies higher than 2–4 MHz, and regions of LF dispersion in the frequency range 0.5–1 MHz. Low-frequency dispersion of this type was observed mostly in films of calcium-germanium garnets. In samarium-gallium garnets the low-frequency dispersion is much weaker. The regions of LF dispersion for several typical calcium-germanium iron-garnet samples, whose parameters are indicated in the table, are shown in greater detail in Fig. 2. We have interpreted the LF dispersion of the spectra, which has the characteristic shape of a "step," as a manifestation of the magnetic aftereffect which is well known for strongly anisotropic ferrites⁷ and is caused by relaxation of the induced anisotropy in the course of DW motion.

TABLE I. Parameters of calcium-germanium iron-garnet films (h —thickness, $\chi_0 = 4\pi\partial M/\partial H$ —magnetic susceptibility of domain structure, $\partial x/\partial H$ —structural susceptibility, $4\pi M_s$ —saturation magnetization, Q —quality factor, $\delta = \pi(A/K)^{1/2}$ —domain-wall thickness, $x_0 = (\partial x/\partial H_0)H_0$ is the static amplitude of the DW displacement.

Sample No.	h , μm	$4\pi M_s$, G	Q	χ_0	$\partial x/\partial H$, $\mu\text{m}/\text{Oe}$	δ , μm	x_0 , μm	η	W_0 , erg/cm^3	τ , μsec
1	9.4	141	10.0	1.357	0.0283	0.074	0.110	0.036	2.1	0.21
2	5.3	200	9.3	1.662	0.0194	0.083	0.112	0.064	8.6	0.20
3	6.5	180	9.0	1.730	0.0291	0.116	0.113	0.110	12.6	0.24
4	3.0	120	7.85	3.231	0.0937	0.186	0.365	0.176	6.7	0.33

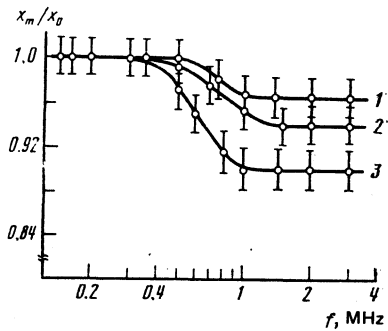


FIG. 2. Detailed form of the dispersion sections of the low-frequency spectra. The numbers at the curves correspond to the numbers of the samples in the table.

It is known that the crystal magnetic energy due to contributions from the crystallographic energy, from exchange, and from dipole and exchange fields is a minimum at a definite spatial distribution of the magnetization, and this leads to formation of a stable domain structure. In the case, however, of a nonideal crystal that contains, e.g., impurities, the total energy depends also on the local ordering of these impurities over crystallographically equivalent positions of the crystal lattice, and this ordering is determined in turn by the local orientation of the magnetic moment.⁵⁻⁷ The presence of a domain structure causes a statistical diffusional regrouping of the impurities over these energetically nonequivalent positions of the crystal lattice, and a spatially inhomogeneous distribution of their concentrations sets in, leading thereby to an additional decrease of the total magnetic energy of the crystal. As a result, an additional stabilization of the existing domain structure takes place. In other words, minimization of the magnetic energy of a nonideal crystal is determined not only by the "global" contributions from the anisotropy, exchange, and other energies, which determine the large-scale distribution of the magnetization (the domain structure), but also by small contributions due to the ordering of the impurities. As a rule these contributions are small and cannot compete with the main contribution to the magnetic energy, meaning that they cannot change the existing domain structure. This additional energy, which stabilizes the domain structure (domain walls) is interpreted as the induced-anisotropy energy. We follow here Néel's simple phenomenological treatment,⁵ according to which a diffuse distribution of the impurity produces in the vicinity of each DW a local induced anisotropy that pins the DW in the initial static-equilibrium position, and this is equivalent obviously to the formation of a potential energy trap in the vicinity of DW, which prevents the latter from moving away from the initial position. Another consequence of the induced anisotropy are the MA due to impurity relaxation in DW displacements.

We consider now the influence of induced anisotropy on the dynamics of small DW oscillations. According to Refs. 5 and 7, at small DW displacements the exact problem of the interaction of a moving DW with a self-consistent stabilizing potential $W_s(x,t)$ reduces to the simpler quasi-static problem of the interaction of a "rigid" undeformable potential $W_s(x)$ with a DW, and the dynamics of the poten-

tial W_s itself is described in the approximation of a kinetic equation analogous to the kinetic equation for an impurity density $n(x,t)$ with a single relaxation constant τ . The energy of the interaction of the DW with the relaxing impurity atmosphere is of the form

$$P(x,t) = - \int_{-\infty}^t \frac{\partial W_s(x-x')}{\partial x} \frac{\exp[-(t-t')/\tau]}{\tau} dt'. \quad (1)$$

(For the considered case of 180-deg domain walls, the calculations of the spatial configuration of the stabilizing barrier $W_s(u)$ are given in Refs. 6 and 11.)

It follows from the experimental data (Fig. 1) that in the region of the frequencies of the DW oscillations, where the MA manifests itself, the inertial effects of the DW and the influence of the viscous damping of the DW motion can be neglected. Therefore, in the quasistatic approximation that is valid here, the DW motion under the influence of a weak harmonic field $H(t) = H_0 \exp(i\omega t)$ is determined by the balance of the force of the magnetic pressure of the external field $2M_s H(t)$, of the quasielastic force $-kx(t)$, where $k = 2M_s/(\partial x/\partial H)$, due to the local demagnetizing field of the stripe-domain structure or to the external gradient, and of the force $P(x,t)$ of the stabilizing barrier:

$$kx(t) - P(x,t) = 2M_s H(t). \quad (2)$$

The solution of the Volterra integral equation (2) is given in Ref. 8 and determines the normalized frequency spectrum of small oscillations of a DW that interacts with the relaxing atmosphere of the impurity⁷:

$$\frac{x_m}{x_0} = \left[\frac{1 + \omega^2 \tau^2}{1 + \omega^2 \tau^2 (1 + \eta)^2} \right]^{1/2}, \quad (3)$$

where $x_0 = 2M_s H_0/k$ is the static amplitude of the DW displacement ($\omega = 0$), x_m is the dynamic amplitude, $\eta = aW_0/k\delta$ is the dimensionless energy of the induced anisotropy, $\delta = \pi(A/K)^{1/2}$ is the width of a Bloch DW, and $a \sim 1$ is a numerical parameter.

The frequency spectra calculated from (3) are shown in Fig. 3 for three values of the dimensionless parameter $(1 + \eta)^{-1}$, corresponding to those measured in experiment and shown in Fig. 2 (samples 1-3). Comparison of Figs. 2 and 3 shows good agreement between the experimental and calculated spectra of the DW oscillations. The characteristic spectrum dispersion, the "step" on Figs. 2 and 3, has a simple physical meaning. At low oscillation frequencies

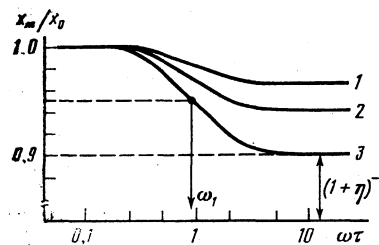


FIG. 3. Amplitude spectra of DW with dispersion section due to the magnetic aftereffect, calculated in accord with Eq. (7) for the values of the parameter $1/(1 + \eta)$ corresponding to those measured experimentally in accord with Fig. 2 (curves 1, 2, and 3).

($\omega \ll \tau^{-1}$) the stabilizing potential (the impurity atmosphere) manages to follow the displacing DW, which continues thus to remain immobile relative to the minimum of the potential W_s and is not subject to retardation by its field. At higher frequencies ($\omega \gg \tau^{-1}$) the kinetic impurity relaxation processes with characteristic time τ do not manage to realign the spatial position of the stabilizing potential: the DW moves relative to the potential, is retarded by its field, and the amplitude of the DW oscillations decreases. In the dispersion region ($\omega \sim \tau^{-1}$) the frequency of the forced oscillations of the DW is comparable with the impurity-relaxation frequency.

It can be seen from Figs. 2 and 3 that the stabilizing potential $W_s(x)$ due to the induced anisotropy is in this case small compared with the potential of the quasielastic force $kx^2/2$ due to the demagnetizing fields of the domain structure, and the MA is small. An idea of the ratios of these quantities is given by the values of the parameter η in the table, which lists also the calculated induced-anisotropy energy W_0 . A comparison of the calculated and experimental spectra makes it possible to determine the constants of the relaxation-time τ from the frequency ω_1 at the half-maximum of the DW oscillation amplitude, namely $\tau^{-1} \approx (1 + \eta)\omega_1$, as shown schematically in Fig. 3 for sample No. 3. For this group of samples, the calculated values of τ were respectively 0.21, 0.20, and 0.24 μsec (see the table). The close values of τ of different samples of the same composition indicate that the MA mechanisms in these iron garnets are identical despite the difference due to the differences in the geometric and magnetic parameters of the samples, in the absolute values of the induced-anisotropy energy W_0 .

It must be emphasized that in these cases we succeeded in separating experimentally well-resolved dispersion sections of the spectra, sections typical of the MA, only because in this frequency band there are no effects of viscous damping and inertia in the DW motion. In those cases when the frequency τ^{-1} of the induced-anisotropy relaxation is comparable with the "natural" relaxation frequency of the DW on account of viscous damping, $\omega_c = k\mu/2M_s$ (μ is the DW mobility), two different dispersion sections are superimposed and the general picture of the spectra becomes more complicated. To analyze the spectra with simultaneous allowance for the viscous damping and MA it is necessary to add in Eq. (2) for the balance of the magnetic-pressure forces a term $\beta x(t)$, where $\beta = 2M_s/\mu$:

$$\beta \dot{x} + kx - P(x, t) = 2M_s H_0 e^{i\omega t}. \quad (4)$$

At low amplitudes of the DW oscillations, approximating as in Ref. 8 the spatial profile of the stabilizing potential in (1) by the parabolic function $W_s(u) \sim W_0 u^2$ of the coordinate u of the displacement relative to its minimum,⁵ we obtain from (4) an integro-differential equation that reduces the usual second-order equation

$$\frac{\beta \tau}{k} \ddot{x} + \left[\frac{\beta}{k} + (1 + \eta)\tau \right] \dot{x} + x = x_0 (1 + i\omega\tau) e^{i\omega t}, \quad (5)$$

whose normalized frequency spectrum is of the form

$$\frac{x_m}{x_0} = \left[\frac{1 + q^2 y^2}{(1 - qy^2)^2 + y^2 [1 + q(1 + \eta)]^2} \right]^{1/2}. \quad (6)$$

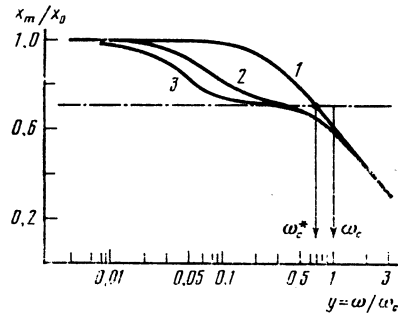


FIG. 4. Amplitude spectra of DW oscillations with simultaneous allowance for the MA and the viscous damping; the spectra were calculated from relation (9) for $q = 1$ (curve 1), $q = 10$ (curve 2), and $q = 20$ (curve 3) at a fixed value of the parameter $\eta = 0.2$.

(we have used here the notation $y = \omega/\omega_c$ and $q = \tau\omega_c$.)

Figure 4 shows plots of Eq. (6) for the "mixed" spectra of the DW oscillations, which are typical of weak MA ($\eta \ll 1$), at different values of the parameter $q = \tau\omega_c$, which is the ratio of the DW natural relaxation frequency ω_c , due to viscous damping, to the impurity relaxation frequency τ^{-1} . It can be seen that at large differences between these frequencies ($q = 10$, curve 2, and $q = 20$, curve 3) the spectrum dispersion section that correspond to these effects do not overlap and are well resolved. At close values of these frequencies ($q = 1$, curve 1), however, the dispersion step of the MA is completely smoothed out by the intrinsic relaxation falloff of the spectrum, and it impossible to resolve the dispersion of the MA experimentally. We note that in the described situation where the dispersions overlap, the general form of the spectrum of the DW oscillations is in fact the same as the typical relaxation relation (Fig. 5), but with a shift of the "effective" relaxation frequency ω_c^* (determined experimentally at the $1/\sqrt{2}$ level of the oscillation amplitude towards lower frequencies. This shift is particularly noticeable at large MA ($\eta > 1$).

Figure 6 shows plots of the shift of the effective relaxation frequency relative to the true one, ω_c^*/ω_c , vs the frequency ratio $q = \tau\omega_c$ for different dimensionless energies of the induced-anisotropy η . Since the widely used experimental procedure of measuring the mobility μ of a DW ($\mu = (2M_s/k)\omega_c$) is based on measurement of the relaxation frequency of the DW oscillation spectrum,^{13,14} where only the effect of the viscous damping is considered, it is clear that

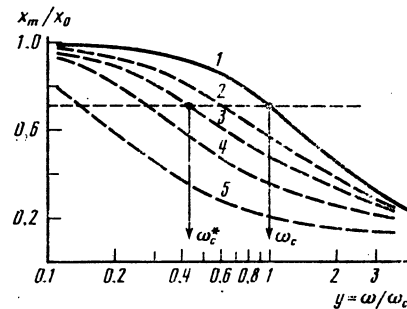


FIG. 5. The same as Fig. 4, for a fixed parameter $q = 1$ at different values of the MA: 2 - $\eta = 0.5$, 3 - 1, 4 - 2, 5 - 5. Curve 1—usual relaxation effect without MA ($\eta = 0$).

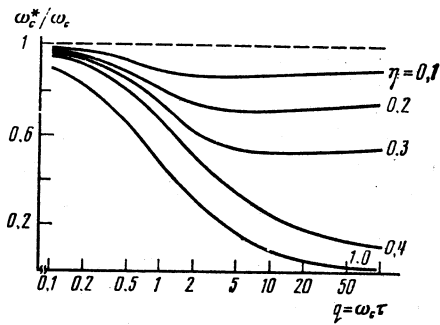


FIG. 6. Change of the effective frequency ω_c^* vs the ratio q of the frequencies of the intrinsic relaxation and of the relaxation of the impurities for weak ($\eta < 0.3$) and strong ($\eta > 0.4$) magnetic after effects, calculated in accord with Eq. (9).

because of the presence of large MA the quantity measured is not the intrinsic but of the effective relaxation frequency ω_c^* of the spectrum, which can differ from ω_c (Fig. 6) and thus underestimate the DW mobility in real samples.

The observed situation can be observed for orthoferrites, whose DW oscillation-spectrum relaxation falloff is in the lower-frequency range 0.1–2.0 MHz (Ref. 14). We have measured carefully the DW-oscillation spectrum in a sample of yttrium orthoferrite (YFeO₃) grown by crucibleless zone melting,¹⁵ see Fig. 7. It can be seen that the spectrum has the typical relaxation-falloff form, although it does not agree exactly with the calculated form $\sim(1 + y^2)^{-1/2}$ of the pure relaxation spectrum. The measured relaxation frequency is $\omega_c^* = 2\pi \cdot 0.505$ MHz, giving for the DW mobility of this sample $\mu = 4100$ cm/sec·Oe. Numerous published data on the DW mobility in YFeO₃, including some obtained by the indicated method, yield greatly varying values of μ from 2200 to 6800 cm/sec·Oe and higher.^{14,16} In connection with the foregoing there are grounds for assuming that the differences of the spectra from the purely relaxational ones and the large scatter of the DW mobility are due to the different degrees purity and of impurity density of the different samples, which produce induced anisotropy and lead to MA that manifest themselves as additional dissipation of the DW energy and distortion of the spectra.

4. DEDUCTIONS AND CONCLUSION

It must be emphasized that investigations of MA in magnetic materials are usually carried out by measuring the integral magnetic susceptibility of the entire sample as a whole,⁷ but the absence of exact information on the sample domain structure (especially in the case of optically opaque polycrystalline materials) leaves open the question of the relative contributions made to the susceptibility to the MA of the rotation processes as well as by the motion of the DW when the magnetization of the sample is reversed. In the case considered here, that of thin single-crystal iron-garnet films with perpendicular anisotropy, having an irregular domain structure, magnetization reversal in weak fields is due exclusively to DW motion. Therefore the magneto-optical procedure used in the present study to record the susceptibility by picking off a signal from a DW makes it possible to investigate in detail. The MA that appear when DW move in local

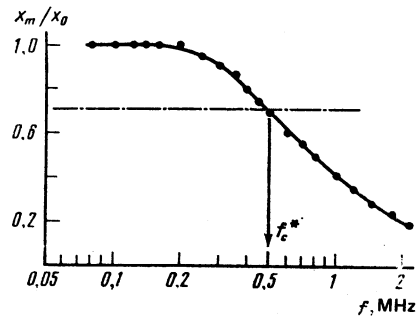


FIG. 7. Measured spectrum of small DW oscillations in YFeO₃ sample.

sections of the sample, and the independently measured magnetic parameters of the material and the characteristics of the domain structure make it possible to compare the experiment with the corresponding phenomenological models.

It must be noted that our phenomenological description of the MA of a moving DW^{5,8} does not specify the induced-anisotropy relaxation mechanism itself. The published data⁷ on induced anisotropy and MA in iron garnets are frequently contradictory. Among the discussed relaxation mechanisms, the most probable are assumed to be diffusion migration of impurity ions and ion vacancies in the garnet lattice, as well as exchange of valence of electrons of the ions, $\text{Fe}^{3+} \leftrightarrow \text{Fe}^{2+}$ (electron diffusion). In the given case of calcium-germanium iron garnets the latter valence-exchange mechanism can apparently also take place because of the presence of divalent calcium ions and tetravalent germanium ions, which can play the role of activation centers that initiate the electron exchange in samples of not strictly stoichiometric composition, as is the case for silicon-doped yttrium iron garnet,¹⁷ where the role of the activation centers is placed by the Si^{4+} impurity ions. To identify the real relaxation mechanism in each concrete composition it is necessary to determine the activation energy of the process \mathcal{E} , and this calls for temperature investigations. Nevertheless, typical values of the activation energy of the process $\text{Fe}^{3+} \leftrightarrow \text{Fe}^{2+}$ in ferrites are tenths of an electron volt ($\mathcal{E} = 0.17$ eV for $\text{Y}_3\text{Fe}_{5-x}\text{Si}_x\text{O}_{12}$, Ref. 17), whence, using our measured values of the relaxation time $\tau(300 \text{ K}) \sim 10^{-7}$ sec, we obtain from the expression $\tau = \tau_\infty \exp(\mathcal{E}/kT)$ an estimate of the impurity relaxation frequency $\omega_\infty = \tau_\infty^{-1}$, corresponding to infinite temperature and $\omega_\infty \sim 10^{10} \text{ sec}^{-1}$, which is of the order of the corresponding frequencies for single-crystal ferrites containing Fe^{2+} ions,⁷ with a predominant electronic valence exchange mechanism.

In real samples, the dispersion magnetic aftereffects can be due simultaneously to several mechanisms, including thermally activated microdefects of the crystal lattice and large impurity clusters,¹⁻⁴ particularly on the film-substrate interface. The corresponding "relaxation" frequencies in the region of the characteristic steplike dispersion of the electrons in samples with large defect density has characteristic values $\tau^{-1} = 10^2\text{--}10^4 \text{ sec}^{-1}$ (Ref. 3), which is less by several orders of magnitude than the characteristic induced-anisotropy relaxation frequencies measured by us.

The presence of a magnetic aftereffect in YFeO₃, due to the electron exchange $\text{Fe}^{2+} \leftrightarrow \text{Fe}^{3+}$, was observed by Ikuta

and Shimidzu,¹⁸ who obtained a rough estimate $\tau \sim 10^{-8}$ sec for the relaxation time. Calcium ions were observed in the samples.

The authors take the opportunity to thank K. V. Valiev and A. K. Zvezdin for a discussion of the results and valuable remarks that led to improvements in the present paper, and V. K. Raev for support. The authors thank A. M. Balbashov for kindly supplying the orthoferrite samples and A. K. Baranov for supplying the iron-garnet film samples.

¹B. Barbara, J. Magin, and H. Jouve, *Appl. Phys. Lett.* **31**, 133 (1977).

²S. Shiomi, S. Iwata, S. Uchiyama, and T. Fujii, *IEEE Trans., MAG-15*, 930 (1979).

³I. G. Avaeva, F. V. Lisovskii, and V. I. Shcheglov, *Fiz. Tverd. Tela (Leningrad)* **20**, 2051 (1978) [*Sov. Phys. Solid State* **20**, 1184 (1978)].

⁴T. Egami, *Phys. Stat. Sol. (a)* **19**, 747, 157 (1973).

⁵L. Néel, *J. Phys. Rad.* **13**, 249 (1952).

⁶S. Taniguchi, *Si. Rep. RITU A8*, 173 (1956).

⁷S. Krupicka, *Physics of Ferrites (Russ. transl.)*, Vol. 2, Mir, 1976.

⁸S. Krupicka and V. Rosovec, *Czech. J. Phys.* **B16**, 99 (1966).

⁹J. F. Janak, *J. Appl. Phys.* **34**, 3356 (1963).

¹⁰B. E. Argyle and A. P. Malozemoff, *AIP Conf. Proc.* **10**, 344 (1973).

¹¹R. Shaw, J. Moody, and R. Sandford, *J. Appl. Phys.* **45**, 2672 (1974).

¹²R. Shaw, D. Hill, R. Sandfort, and J. Moody, *J. Appl. Phys.* **45**, 2346 (1973).

¹³P. W. Shumate, *IEEE Trans. MAG-7*, 586 (1971). J. A. Cape, *J. Appl. Phys.* **43**, 3551 (1972).

¹⁴F. S. Rossol, *J. Appl. Phys.* **40**, 1082 (1969). I. Tomas, *Phys. Stat. Sol. (a)* **30**, 587 (1975).

¹⁵A. M. Balbashov, A. Ya. Chervonenkis, A. V. Antonov, and V. E. Bakh-teuzov, *Izv. AN SSSR, ser. fiz.* **35**, 1243 (1971).

¹⁶G. R. Woolhouse and P. Chaudhari, *AIP Conf. Proc.* **18**, 247 (1974).

¹⁷R. P. Hunt, *J. Appl. Phys.* **38**, 2826 (1967).

¹⁸I. Ikuta and R. Shimidzu, *J. Phys. D; Appl. Phys.* **7**, 726 (1974).

Translated by J. G. Adashko